NJC

ROYAL SOCIETY OF CHEMISTRY

PAPER

View Article Online
View Journal | View Issue

Cite this: *New J. Chem.*, 2021, **45**, 7830

Toward an efficient and eco-friendly route for the synthesis of dimeric 2,4-diacetyl phloroglucinol and its potential as a SARS-CoV-2 main protease antagonist: insight from *in silico* studies†

Triana Kusumaningsih, * Wahyu E. Prasetyo, Fajar R. Wibowo and Maulidan Firdaus

Received 16th December 2020,
Accepted 31st March 2021

DOI: 10.1039/d0nj06114j

rsc.li/njc

As a consequence of the unavailability of an anti-viral drug for SARS-CoV-2, the prospect of developing an antiviral drug is of great importance in this current emergency of the COVID-19 pandemic era. To support the enduring research on the improvement of COVID-19 therapeutics, herein, we demonstrated the development of highly effective and eco-friendly synthetic routes for the synthesis of dimeric 2,4-diacetyl phloroglucinol **4a**, a potent antibiotic and malarial drug candidate *via* phenol–aldehyde condensation over silica sulphuric acid (**SSA**) catalyst and the arylation of dimethylammonium salts under greener protocols, *i.e.*, ultrasound-assisted (US) and liquid assisted grinding (LAG) methods. Through an environmental assessment, the cleanness and environmental efficiency of the developed protocols were evidenced to be improved compared with a recently published alternative synthetic pathway, which was indicated by the presence of higher efficiency and lower environmental impact. In addition, we accomplished molecular docking studies to permit the rapid screening of possible therapeutic ligands of **4a** and its derivatives along with N3, Chloroquine, and Remdesivir as references against the crystal structure for the recently released 3-chymotrypsin-like cysteine protease (**3CL^{pro}**) of SARS-CoV-2. Exclusively, our finding showed that compound **4d** with an excellent binding affinity of −8.1 kcal occupies the active site in varying ways at the N3 binding site of **3CL^{pro}**, confirming its fitness as a good candidate for the therapeutic action against COVID-19. Furthermore, molecular target prediction, pharmacokinetic studies, prediction of the activity spectra for substances (PASS), density-functional theory (DFT), and the structure–activity relationship (SAR) analysis were also established to highlight the prominence of this chemical scaffold.

Introduction

The current 2019-nCoV outbreak has now become a global pandemic, killing hundreds of thousands of people by presenting symptoms linked with fatal respiratory illness.[1–3] According to worldometer data (www.worldometers.info), the cumulative number of confirmed cases around the world has reached 112 263 225 confirmed cases, including 2 485 386 deaths as of 23 February 2021. However, to date, there is no specific drug that has been discovered for this severe and highly contagious viral disease.[4] Thereby, since the first publication on February 2020 of the **3CL^{pro}** crystal structure of SARS-CoV-2,[5] many efforts have been devoted to examining various approved drugs from FDA and secondary metabolites derived from natural products in inhibiting this protein under molecular docking analysis.[6–9]

Over the past decade, the role of natural products in inspiring drug discovery has become exceptionally important.[10,11] It is worthy to mention that there are many studies that have revealed the utilization of bioactive compounds derived from natural products as novel candidate inhibitors against SARS-CoV-2.[12,13] Amongst these, phenolic compounds have been frequently revealed to have good binding affinity with **3CL^{pro}**. Among a large number of the varieties of natural products, phloroglucinol and its derivatives, both natural and synthetic analogues, represent a promising class of phenolic compounds that offers a key structural unit in a large number of favorable pharmacological potentials.[14]

As a privileged phenolic compound, the dimeric 2,4-diacetyl phloroglucinol **4a** (Fig. 1) and its derivatives constitute one of

Department of Chemistry, Faculty of Mathematics and Natural Sciences, Sebelas Maret University, Jl. Ir. Sutami No. 36A, Surakarta, 57126, Indonesia.
E-mail: triana_kusumaningsih@staff.uns.ac.id

† Electronic supplementary information (ESI) available. See DOI: 10.1039/d0nj06114j

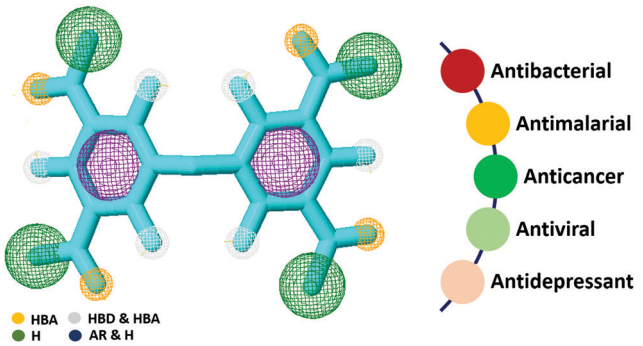

Fig. 1 Pharmacophoric features of **4a** labelled as follows: hydrogen bond acceptor (HBA), hydrogen bond donor (HBD), hydrophobic (H), and ring aromatic (AR) and its reported biological activities.[15–20,23–26]

the most pivotal derivatives of the acylphloroglucinol class due to their enormous potential as anticancer and antiviral agents. For instance, the synthesized **4a** and its derivatives were reported to be active against various cancer cell lines (Calu1, ACHN, Panc1, HCT116, and H460)[15] and have anti-HIV activity,[16,17] with promising properties as preclinical candidates. In addition, there is a plethora of reports that have revealed the potential of **4a** and its derivatives, both natural and synthetic, as antibacterial, antimalarial,[18] and antidepressant therapeutics.[19] Its structure comprises two-unit monomers of diacylphloroglucinol, which are linked by the methylene bridge containing four pharmacophore features, *i.e.*, hydrogen bond acceptor (HBA), hydrogen bond donor (HBD), and hydrophobic (H) and ring aromatic (AR), as illustrated in Fig. 1.[15,20] Despite its magnificent potential applications, a truly practical and convenient route for the synthesis of **4a** has not been published to date. Recently, several efforts have been devoted to establish various synthetic routes toward **4a** and its derivatives,[15,17,19,21] as presented in Scheme 1. Generally, it was synthesized either *via* condensation between diacylphloroglucinol (DAPG) and an aldehyde as a methylene source with the presence of either homogenous acid or base as a catalyst and several amounts of solvent under varied conditions. However, most of these techniques face certain several difficulties, *i.e.*, low yields of products, the necessity of long reaction time and high temperature, along with the use of non-recyclable catalysts. Besides, recently, full attention has been paid by both the academic and industrial chemical communities in pursuing more sustainable synthetic pathways that are in agreement with the green chemistry principles.[22] As a consequence, the development of a new approach with these parameters for a facile, atom-efficient, and eco-friendly route is highly desirable, in line with the goal of sustainable technology and organic transformations.

In this regard, searching for more practical and eco-friendly alternative protocols for the synthesis of **4a**, we considered combining solid catalysts, namely, silica sulphuric acid (H_2SO_4–SiO_2) or commonly shortened as **SSA**,[27] and other sustainable synthetic techniques, such as ultrasound-assisted (US) and liquid-assisted grinding (LAG) method. Recently, enormous attention has been paid to the development and utilization of

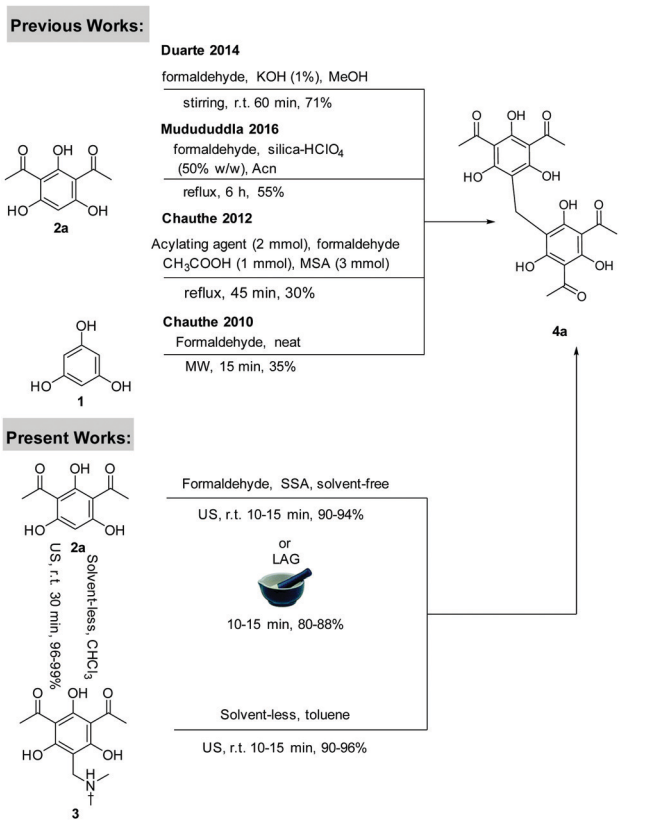

Scheme 1 Various selected literatures for the synthesis of **4a**.[15,17,19,21]

heterogeneous catalysts for promoting various organic transformations due to their outstanding benefits and eco-friendly nature.[28–31] The development of the US method for promoting chemical transformation has become a great growing interest lately. The US method provides high product yields, improved selectivity, easier operation methods, and faster reaction along with waste reduction.[32,33] In addition, since the discovery that the addition of a small amount of solvent or solvent-less conditions can enhance and expose new reactivity of the mechanochemical reaction, the methodology termed as liquid = assisted grinding (LAG) or solvent-drop grinding[34–36] has recently become increasingly in demand for breakthrough reactivity competing with that of conventional solution-based reactions.[37]

As part of our continuation in response to the necessity of following green chemistry principles for the synthesis of naturally occurring phloroglucinol derivatives,[31,38–40] in this work, we demonstrated **SSA** as a highly efficient and eco-friendly catalyst for the synthesis of **4a**, which utilizes sustainable methods such as ultrasound-assisted (US), grinding under solvent-free, or LAG methods. Furthermore, to meet the green chemistry principles for the synthesis of **4a**, an environmental assessment was demonstrated using the EATOS software,[41] Andraos's algorithm,[42] and energy calculation metric.[43] Herein, for the first time, we also identified the potential inhibitors of the synthesized compound **4a** and its derivatives using molecular docking to the **3CL^{pro}** enzyme, which is crucial in the management of SARS-CoV-2. Moreover, molecular docking was also performed to test N3 as a native

inhibitor of the **3CL^{pro}** and the FDA-approved antimalarial drug Chloroquine and antiviral drug Remdesivir to provide a comparison with the binding stability of these synthesized compounds.

Experimental

Materials and instrumentation

All the reagents and solvents were purchased from Merck or Sigma-Aldrich and utilized without additional purification. Branson B1510R-DTH Ultrasonic Cleaner was used to perform any reactions under sonication condition. Silica gel with pore size of 60 Å, 230–400 mesh was used to perform column chromatography. Thin Layer Chromatography (TLC), which was performed on gel 60 F_{254} (Merck) plate, was used to monitor the progress of the reactions. UV light at λ = 254 and 365 nm was used for the visualization of the TLC spot. Agilent DD2 Nuclear magnetic resonance (NMR) spectrometer was used to record the NMR spectra, 500 MHz for ^{1}H and 125 MHz for ^{13}C using $CDCl_3$ as the solvent, operated at 25 °C using tetramethyl silane as the internal standard. All of the collected spectra are shown in ESI S2 (ESI†). Melting Point Apparatus SMP10 Stuart was used to measure the melting points of the isolated product.

Preparation of the SAA catalyst

The catalyst was prepared following the procedure from the previous work.[44] 12.375 g of silica gel was soaked in 50 mL of diethyl ether (Et_2O) and 6.25 mmol of concentrated H_2SO_4. The obtained mixture was stirred for 15 min at ambient temperature and pressure under atmospheric nitrogen (N_2) and dried at 60 °C for 18 h. The solvent in the resultant residue was then removed by heating at 120 °C for 6 h. Finally, before further use, the resultant **SSA** catalyst was placed in a desiccator for storage.

General procedure for the synthesis of 2,4-diacylphloroglucinols (2a–2c)

The synthesis of monomeric 2,4-diacylphloroglucinols was performed by following the previous work.[44] To the round bottom flask, phloroglucinol **1** (1 mmol) and acetic anhydride or acyl chlorides (2 mmol) were stirred at ambient temperature and pressure for 5 min. Then, into the mixture, 20% (w/w) **SSA** was added as a catalyst and sonicated at 60 °C for 15–20 min. Upon reaction completion, the mixture was cooled to 25 °C, diluted with 15 mL of water, and extracted with ethyl acetate (EtOAc) (3 × 15 mL). Finally, the solvent was evaporated and the crude product was subjected to further purification through short flash column chromatography using *n*-hexane/EtOAc (95/5 → 70/30 gradient) in silica gel.

General procedure for the synthesis of 4a *via* the condensation reaction

In a vial, monomer **2a** (0.1 mmol), formaldehyde (0.5 mmol), and **SSA** (20%) were placed. The resultant mixture was reacted under ultrasound irradiation. The reaction typically took 10–15 min, which was monitored by TLC. Upon completion of the reaction, 4 M hydrogen chloride (HCl) was used to neutralize the crude solution. EtOAc (3 × 10 mL) was then used to extract the aqueous layer. The combined organic layers were dried over sodium sulphate anhydrous (Na_2SO_4). Finally, the solvent was removed and the crude product was collected and used without further purification.

General procedure for the synthesis of 4a *via* one-pot synthesis using Eschenmoser's salt

To a round bottom flask, a solution of the monomer of diacylphloroglucinol **2a** (0.1 mmol) and the suspension of Eschenmoser's salt[45,46] (0.5 eq.) was heated at 60 °C in a small amount of chloroform ($CHCl_3$) under the US method in N_2 atmosphere. The obtained mixture was refluxed until most of diacylphloroglucinol converted to the desired product. To the obtained mixture, 5 mL dichloromethane (CH_2Cl_2) was then added and gently washed with 5 mL of 1 N aqueous HCl and brine solution. CH_2Cl_2 (3 × 5 mL) was used to extract the resultant aqueous layer. The combined organic layers were dried over magnesium sulphate anhydrous ($MgSO_4$), filtered with filter paper, and evaporated using a rotary evaporator. The obtained crude residue was purified by short flash chromatography using n-hexane/EtOAc (95/5 → 80/20 gradient) in silica gel.

Arylation of dimethylammonium salt 3

A solution of the desired acylated phloroglucinol **2a** (1.0 eq.) was reacted with the corresponding dimethylaminomethylated monomer (1.0 eq.) using a small amount of toluene under US method at room temperature until most of the acylated phloroglucinol was converted to the expected product. Upon completion of the reaction, the solvent was removed. Finally, before further use, CH_2Cl_2 was used to wash the crude product.

General synthesis of 4a *via* arylation of dimethylammonium salt

A solution of diacylphloroglucinol monomer **2a** (1.0 eq.) with the activated dimethylammonium salts from monomer **3** (1.0 eq.) was heated at 80 °C in a small amount of toluene for a designated time. The solvent was then removed and the crude product was collected and used without further purification.

Reusability and heterogeneity of the SSA catalyst

After the completion of the reaction, the collected **SSA** catalyst was stirred in 10 mL of EtOAc for 5–10 min. Then, it was filtered and washed with 5 mL of EtOAc and acetone, respectively. After that, before further use, the filtered catalyst was dried at 120 °C for 3 h. In addition, hot filtration was performed following the previous methods[44] to observe the possible leaching of **SSA** active sites.

Environmental assessment

To assess the environmental impact of the present method, the combination between the Environmental Assessment Tool for Organic Syntheses (EATOS) software established by Eissen and Metzger[41] and the algorithm by Andraos[42] was performed. The necessitated data related to their detail of stochiometric data was attained from the recent literatures[15,17,19,21] both for EATOS and the Andraos algorithm. For further details about the

energy efficiency profile, the energy calculation measurement established by Clark and co-workers[43] was accomplished. As a note, the details of the workup and purification stages are not included in this assessment due to the lack of procedural information.

Preparation of protein targets $3CL^{pro}$ and ligands

The X-ray crystallographic structures of $3CL^{pro}$ in the complex with the inhibitor N3 was retrieved from the Protein Data Bank database with PDB ID: 6LU7 (htttp://www.rscb.org/); then, chain A was loaded into the AutoDock Tools (version 1.5.6) software. Through this software, the ligand N3, water, and ions molecules were removed. PrankWeb (http://prankweb.cz/) was used to identify the active sites of the selected receptors. Finally, before the docking studies were performed, polar hydrogen atoms and Gasteiger charges were added.

Density-functional theory (DFT) studies

All of the studied compounds were sketched with PerkinElmer Informatics ChemDraw (version 17.1). The quantum chemical calculation for all the investigated molecular structures was carried out in GAUSSIAN 09 suite of programs. The optimization of all the stationary points of the desired molecules was done using the 6-31G (d,p) basis set with the Lee–Yang–Parr exchange–correlation (B3LYP) density functional in the gas phase. It allows calculating the values of the orbital energy HOMO and LUMO, total energy, gap energies (ΔE_{gap}), and several other molecular electronic properties.[47,48] In addition, molecular electrostatic potential (MEP) calculation derived from Mulliken charge was performed to access the detailed information of the nucleophilic and electrophilic sites.

Molecular docking studies

Molecular docking has been extensively used in structure-based drug design.[7] To assess the binding difference between the synthesized **4a** and its derivatives along with N3, Chloroquine, and Remdesivir as the references with the $3CL^{pro}$, a comparative molecular docking analysis was performed using the PyRx software by the AutoDock wizard.[49] The interactions between the receptor and the result of the concerned ligands were compiled, visualized, and analyzed using PyMol (version 1.7.4) and BIOVIA Discovery Studio Visualizer 2020.

Molecular target prediction

The synthesized **4a** and its derivatives may interact with several proteins, or bind to proteins or other macro-molecular targets. Accordingly, it is essential to predict the molecular targets for these investigated molecules. It can be easily investigated using the accessible free-of-charge Swiss Target Prediction (http://www.swisstargetprediction.ch/index.php).[50]

Drug-likeness prediction and ADMET analysis

Drug-likeliness properties of the ligands were assessed using SwissADME (http://www.swissadme.ch/). The ADMET (*i.e.*, absorption, distribution, metabolism, excretion, and toxicity) analysis was accessed using admetSAR (http://lmmd.ecust.edu.cn/admetsar1) and *pKCSM* approach (http://biosig.unimelb.edu.au/pkcsm/).[51]

Prediction of the activity spectra for the substances (PASS)

The prediction of activity, particularly antiviral activities of **4a** and its derivatives, were assessed using PASS (http://www.way2drug.com/). This is an accessible free-of-charge computer program, which can estimate the activity of molecules.[52]

Results and discussion

Chemistry

Synthesis of 4a derivatives. In the first endeavor, we commenced this investigation on the condensation between two monomers of 2,4-diacetylphloroglucinol (DAPG) **2a** using formaldehyde as the linker under different reaction conditions, as presented in Table 1. The retrosynthetic analysis depicts that compound **4a** can be proposed by the joining of two monomeric DAPG units through a methylene linkage, as represented in Scheme 2.[17]

The used monomers were synthesized according to the previous literature,[44] as depicted in Scheme 3. To carry out this phenol–aldehyde condensation reaction, various catalysts were examined. A quick analysis of Table 1 revealed that this typical reaction proceeded smoothly in the existence of catalyst, either basic or acidic, to give the desired product **4a** in moderate to high yields in all the methods, *i.e.*, oil-bath, stirring, and US condition. It has appeared that in this typical reaction, the catalyst shows a dominant role in ensuring efficient reaction rate and yields, which was ascertained by the fact that no product formed or lower yield was detected in the absence of any catalyst under the three different methods (oil-bath, stirring, and US method) even after prolonged reaction times.

Among the catalyst used, carrying out the reaction in the presence of homogenous acid catalysts like acetic acid (AcOH), H_2SO_4, HCl, and methanesulfonic acid (MSA) furnished the product in low to moderate yields under both the reaction conditions (Table 1). Nevertheless, the expected product was found to be in slightly higher yield under the US method compared to the yield of the reflux or stirring method. No product was detected in the presence of weak acid AcOH. The use of strongly acidic such as HCl, H_2SO_4, and MSA furnished low to moderate yield of the desired product **4a**, which ensures further improvement in the yield and a noticeable decrease in the reaction time compared to the AcOH catalyst. Furthermore, the used of the conventional base catalyst 1% KOH[19] was also found to be insignificant in furnishing the expected product. When several organic solvents, such as $CHCl_3$ and methanol (MeOH), were introduced, they were also observed to be inferior in all the cases as compared to the solvent-free condition. However, when $CHCl_3$ was used as a solvent, the expected product yield was higher than that using MeOH. The use of highly polar protic solvent such as MeOH could decelerate the rate of this typical reaction by deactivating the nucleophile *via* HB interactions. Besides, strong dipole moments could also stabilize the negative charge localized on the reactants, which can trigger an enhancement in the activation energy; thereby, the rate of the condensation reaction is decelerated.[53,54]

Table 1 Condensation of two units of DAPG **2a** (1 eq.) using 37% HCHO (0.5 eq.) under different reaction conditions

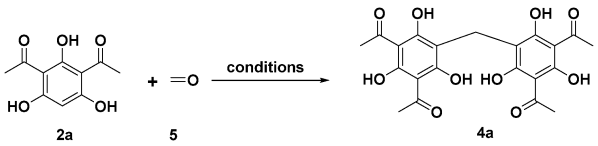

		Oil-bath/classical stirring (r.t.)		US		
Entry	Reagent/solvent	T (°C), t	Yield[a] (%)	T (°C), t	Yield[a] (%)	Solvent ranking[b]
1	Neat	r.t, 6 h	[c]	r.t, 1–2 h	—	nr
2	Solvent-free, ACOH (15 eq.)	r.t, 3 h	[c]	r.t, 1–2 h	<10	nr
3	Solvent-free, conc. H_2SO_4 (10 eq.)	r.t, 3 h	26	r.t, 1 h	35	nr
4	MeOH, conc. H_2SO_4 (10 eq.)	r.t, 6 h	38	r.t, 1 h	44	Recommended
5	MeOH, conc. H_2SO_4 (10 eq.)	64, 4–5 h	49	64, 45 min	52	Recommended
6	Solvent-free, HCl (15 eq.)	r.t, 6 h	<15	r.t, 1 h	21	nr
7	Solvent-free, MSA	r.t, 3 h	35	r.t, 45 min	39	nr
8	$CHCl_3$, MSA	60, 5 h	34	r.t, 30 min	42	Highly hazardous
9	Solvent-free, 1% KOH	r.t, 3 h	45	r.t, 1 h	60	nr
10	MeOH, 1% KOH	r.t, 3 h	75	r.t, 1 h	80	Recommended
11	MeOH, silica gel	r.t, 3 h	[c]	r.t, 1 h	—	Recommended
12	Solvent-free, **SSA** (20%)	r.t, 3 h	44	r.t, 1 h	56	nr
13	MeOH, **SSA** (20%)	r.t, 3 h	38	r.t, 1 h	51	Recommended
14	$CHCl_3$, **SSA** (20%)	r.t, 3 h	47	r.t, 1 h	59	Highly hazardous
15	$CHCl_3$, **SSA** (20%)	60, 3 h	51	60, 1 h	55	Highly hazardous
16	Solvent-less $CHCl_3$, **SSA** (20%)	r.t, 3 h	88	r.t, 15–20 min	94	Highly hazardous
17	Solvent-less $CHCl_3$, **SSA** (20%)	60, 3 h	87	60, 30 min	95	Highly hazardous
18	Solvent-less $CHCl_3$, **SSA** (10%)	r.t, 3 h	54	r.t, 15 min	61	Highly hazardous
19	Solvent-less $CHCl_3$, **SSA** (30%)	r.t, 3 h	75	r.t, 15–20 min	88	Highly hazardous

nr: not reported. [a] Isolated yield. [b] Ranking of solvent with respective to CHEM21 solvent guide of "classical" solvents.[55] [c] No reaction.

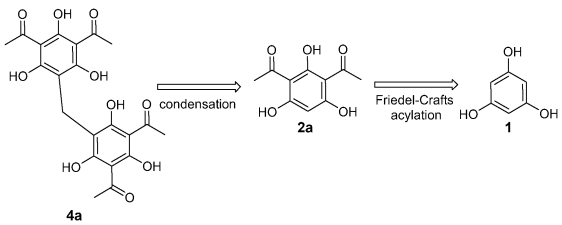

Scheme 2 Disconnection approach to **4a**.

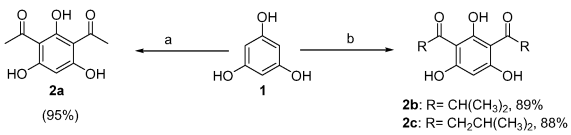

Scheme 3 Reagents and conditions: (a) acetic anhydride (2 mmol), **SSA** (20% w/w), 60 °C, US, 15–20 min, or 80 °C, 30–45 min, (b) RCOCl (2 mmol), **SSA** (20% w/w), 60 °C, US, 15–20 min, or 80 °C, 30–45 min.

Afterwards, we turned to the utilization of heterogeneous Brønsted acid catalyst **SSA** in a similar reaction. Switching the catalyst from a homogenous acid catalyst to a heterogeneous Brønsted acid catalyst **SSA** (20%) was followed by the formation of the product in yields of 44% and 56% when the reaction was performed by conventional stirring and US method using **4a**, respectively. Moreover, increasing the temperature of the reaction to 60 °C caused insignificant conversion to **4a**, which established that heating might not be crucial for the formation of **4a**. To our delight, when performing the solvent-less reaction under solvent-free and room temperature with $CHCl_3$ under conventional stirring and US method, a high yield of **4a** was observed, *i.e.*, 88% and 94%, respectively. With the view of further optimization study, increasing the amount of the **SSA** catalyst to 30% and reducing it to 10%, the yield of **4a** obtained was insignificantly improved on being catalyzed with 20% (w/w) of **SSA**. Therefore, 20% of **SSA** was evidenced as the ideal amount for effective conversion. In order to obtain the investigated catalytic activity of **SSA**, the reaction was also catalyzed using neat silica gel; regrettably, no product formation was observed.

After corroborating the feasibility of the reaction, in our next endeavor, another green alternative method such as LAG[37] was performed. With a small amount of $CHCl_3$ (50 μL solvent/100 mg or η = 0.5), a good yield of 90% of **4a** was successfully isolated after 15–20 min of reaction (Scheme 4). Disappointingly, it was observed that the desired product also formed in low yield (<30%) by the absence of $CHCl_3$ as a solvent. Therefore, the solvent-less condition proved to eb a superior system for the synthesis of **4a** under the US method in the presence of 20% (w/w) of **SSA** at ambient temperature. To validate the reproducibility of the reaction, under similar conditions, this reaction was repeated three times and smoothly furnished the product **4a** in 90%, 90%, and 92% yield, respectively.

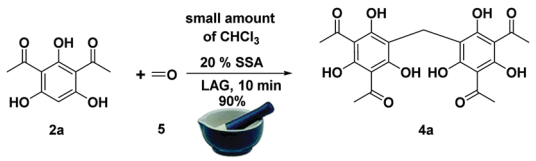

Scheme 4 Synthesis of **4a** under the LAG method.

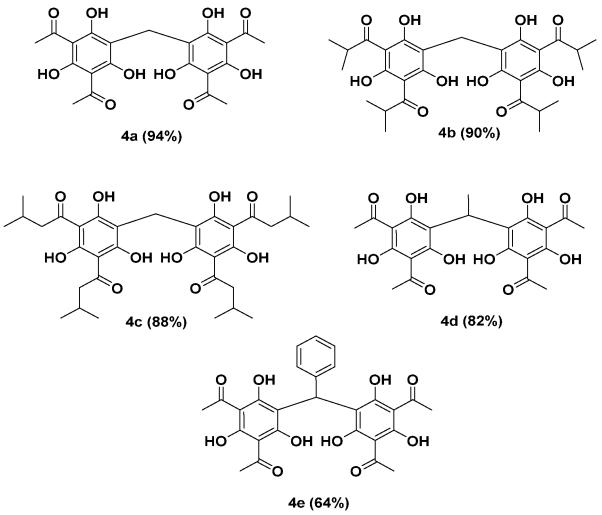

Scheme 5 Substrate's scope of the reaction.

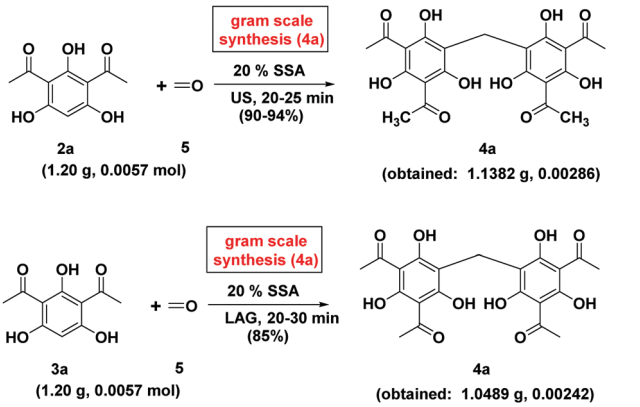

Scheme 6 Preparative scale synthesis of **4a**.

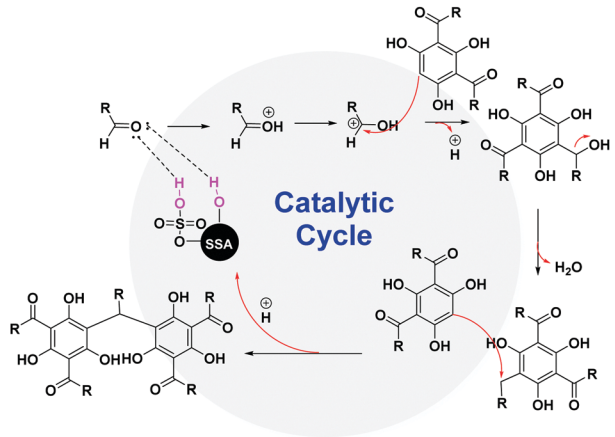

Scheme 7 A plausible mechanism for the formation of **4a** *via* phenol aldehyde condensation.

Substrate scope. As a further effort, under the previously optimized reaction conditions, several of the **4a** derivatives were synthesized with slightly lower yields by the condensation of different acylphloroglucinols and aldehyde (Scheme 5). Incidentally, these reactions were processed forcefully to generate lower yield when the formaldehyde and acetyl chain were replaced with bulkier aldehyde and acylphloroglucinol types. The yield of the targeted products also did not increase even after the reaction time and temperature were increased.

It is worth mentioning that the steric hindrance factor, in consequence of the bulky alkyl chains and/or aldehyde groups, might have significantly affected the selectivity of the product as stated by our previous literatures,[15,17,56] which also investigated the same typical reaction. Therefore, the release of the active methylene intermediate was low. Despite that, the overall yield of compound **4b**, **4c**, and **4d** is still considerable in high yield. Furthermore, an effort to evaluate the role for the formation of heterodimeric between monomer **2a** and **2c** using this accomplished method was also carried out, which was thwarted by the reactivity of the reaction that was only led to the formation of homodimer **4a**.

Scalability. To further highlight the optimized reaction, an experiment of gram-scale phenol–aldehyde condensation of DAPG **2a** and aldehyde was also evaluated. As can be seen in Scheme 6, in the presence of 20% (w/w) **SSA**, the reaction between **2a** and formaldehyde smoothly furnished 1.14 g (92% yield) of the desired product **4a** within 30–40 min of the reaction under solvent-less US condition. Nonetheless, the completion of the scaled reaction under both US and LAG took a slightly longer time as compared to when performed at the mg scale. It can be attributed to the poor heat transfer and insufficient mixing between the reactants and catalyst during the scale-up reaction under solvent-less method. However, in general, compound **4a** could be practically prepared by both the present methods.

Proposed mechanism. Scheme 7 illustrates a plausible mechanistic route for the synthesis of **4a** derivatives *via* phenol–aldehyde condensation. A reasonable first step is the formation of electrophilic species. We hypothesize that an active site of **SSA** activates the aldehyde species by protonating the oxygen atom from the carbonyl group of aldehydes, which produce a partial positive charge of the carbonyl carbon atom (C═O). Thus, the electrophilicity of the carbocation increases. Finally, because of the high level of electron density of diacylphloroglucinols, it will act as a strong nucleophilic species and attack the carbocation of the aldehyde at *ortho–para* to the hydroxyl groups in order to yield the dimeric diacylphloroglucinol.

Reusability of the catalyst. Due to the pressure from both environmental and economic aspects, the recyclability of heterogeneous catalysts is a remarkably critical aspect, particularly for industrial processes. Under the optimized conditions of the reaction, gratifyingly, the desired product and the catalyst can be easily separated only by simple filtration using ethyl acetate after the completion of the reaction and can be used extraordinarily for 7 consecutive runs (Fig. 2). It is worthy to note that the use of an environment- friendly catalyst, low reaction temperature, and the use of solvent-free conditions stand as the main advantages of this present developed method.

Synthesis of 4a using Eschenmoser's salt. After phenol–aldehyde condensation was accomplished, alternatively, we eventually

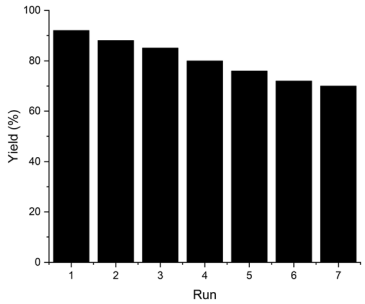

Fig. 2 Yields obtained with recycled SSA on **4a** under optimum condition.

directed to another alternative synthetic strategy of **4a** using Eschenmoser's salt. It was previously reported by Minassi and Appendino, which is a reactive iminium ion and could be an appropriate promoter for the synthesis of arzanol with yield up to 61%.[45]

Another highlight of the utilization of Eschenmoser's salt was also reported by Grayfer *et al.* in 2016 for promoting the synthesis of Mallotojaponin in excellent yields.[46] Reacting **2a** with 0.5 eq. of the Eschenmoser's salt allowed the synthesis of **4a** in 40% yield under solvent-less conventional heating and 56% yield under the US method (Scheme 8). An attempt to improve the yield of **4a** was demonstrated by reacting 3 eq. of Eschenmoser's salt with 1 mmol of **2a**, dimethylammonium salt was exclusively formed, giving **3** in 95% and 99% yield under solvent-less classical stirring and US method, respectively. In line with this, we were also pleased to demonstrate this reaction under the LAG method. Astonishingly, under this greener method, the outcome was somewhat hopeful; we achieved the same product of **4a** in 80% yield after the addition of 100 μL $CHCl_3$/100 mg of monomer (η = 1) after 15–20 min reaction. A comparison between solvent-less magnetic stirring, US, and LAG method implies that the reactions times are more considerably reduced with the US method, which is due to the mechanical effects associated with the sound waves and high reactant concentrations.[57]

Afterward, reacting **3** with 1 eq. of the starting monomer, **2a** could be obtained as the desired product in 80–90% yield after refluxing in toluene for 3–5 h. Meanwhile, when several

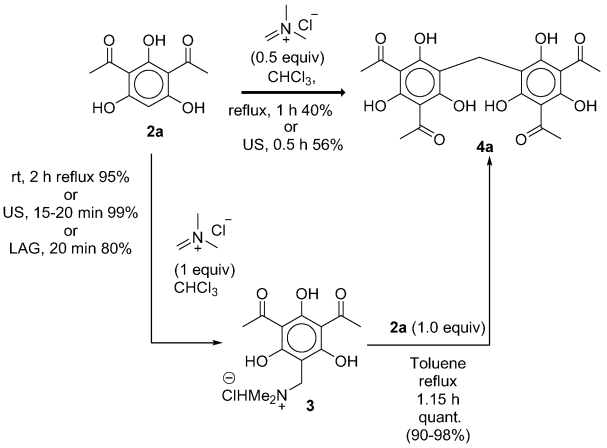

Scheme 8 Synthesis of **4a** using Eschenmoser's salt.

recommended solvents[55] such as EtOH and EtOAc were used in place of toluene, no reaction occurred, which indicated that toluene has an important role in the reaction. Alternatively, the solvent-less reaction was established for the synthesis of **4a** under the US method. Remarkably, the reaction took a shorter time (0.5 h) and the yield was higher (96%) than the reaction with an excess of toluene. It is noteworthy to mention that in this study, solvent-less reaction is superior to the conventional reaction that used a large amount of solvent.

Environmental assessment of the synthetic strategies. In an attempt to assess the sustainability of the synthetic processes of **4a**, we compared the greenness of our developed routes with respect to the existing literatures.[15,17,19,21] As a further effort, we analyzed these procedures, *i.e.*, method A, B, C, D, E, F, G, and H using several green metrics computational tools, EATOS tool[41] and the worksheet developed by Andraos,[42] as presented in ESI S3 and Fig. S1 (ESI†). The EATOS tool takes into account the amount and the nature of substances and waste while the Andraos considers the number of materials involved and waste produced. Since the measurement of energy requirement is not included in EATOS and Andraos evaluation, a straightforward energy calculation established by Clark and co-workers[43] was also demonstrated.

As can be seen in ESI S3 and Fig. S1A (ESI†), both our developed methods, US (method E) and LAG (method F), have a better environmental compatibility factor compared to previously published literatures, which is characterized by the lower value of S^{-1}(mass index), *E*-factor, Ei_{in} (environmental index input), and Ei_{out} (environmental index output) when equal chemistries of the reactions are compared. From the result, it seemed that the present developed methods G and H showed lower environmental profile compared to the methods G and H due to the utilization of the solvent during the reaction. It is worthy to note that the demonstrated phenol–aldehyde based solvent-free or solvent-less condition permitted to an environmental impact factor improvement. In addition, the result obtained from Andraos algorithm also clearly exhibited that the present developed method (Method E) is relatively closer to the ideal conditions, rivaling the other previous reported method or the present developed method (Method F, G, and H) in all the aspects (ESI S3 and Fig. S1B, ESI†).

ESI S3 and Fig. S1C (ESI†) presents the requirement of energy intake for the synthesis of **4a** from all the investigated methods. As we note, because the method F was performed by manual grinding with hand, thus, we excluded the LAG method from the energy intake requirement calculation. The energy consumption of the method E (present method), which was assisted by the US method, was characterized by the lowest energy usage compared to those of previous literatures and the present methods (method G and H). The difference between the energy requirements of methods A and E, however, is less noticeable, in which the two reactions are assisted by the MW and US methods, respectively (the detailed calculation of the requirement of energy intake is given in ESI S4 and Table S1, ESI†). Finally, considering all the used green metrics in this study, it is noticeable that the present developed method (Method E) pointedly enhanced the synthetic strategy for **4a** compared to that of previous literatures.

In silico studies

Molecular target prediction. Initially, we demonstrated molecular target studies, which is a critical key for discovering the potential phenotypes, cross-reactivity or predicting the potential side effects, and optimizing produced by the action of the **4a** derivatives.[50,58] The top 25 of the targets predicted for **4a** derivatives against **3CL^{pro}** of SARS-CoV-2 are shown in ESI S5 and Fig. S3 (ESI†). Astonishingly, all the 5 synthesized compounds have excellent properties of drug ability, which could interact with various classes of enzymes or proteins.

Molecular docking studies. The **3CL^{pro}** main protease is one of the ideal targets for SARS-CoV-2 drug development since it has an important role in controlling the main roles of the virus.[59] Structurally, it comprises a dimeric protein, which holds two symmetric units designated as protomers, which are divided into three domains, (domain I, II, and III) in each of its protomers. The domain III contains five α-helices and is linked with domain II through an extended loop region (residues 185–200). Further, the **3CL^{pro}** has CYS A:145 and HIS A:41 catalytic dyads, and a substrate-binding site is positioned in the cleft between domains I and II (Fig. 3).[59,60]

Through molecular docking, the structural conformations between the active sites of the drug candidate to the desired target are possible to be predicted.[61] Further, molecular docking of **3CL^{pro}** of SARS-CoV-2 was performed on a set of synthesized compounds, *viz.*, **4a–e**, in order to identify the critical ligand–protein interactions. Of note, N3, Chloroquine, and Remdesivir were included as controls. It was observed that all the synthesized ligands had a binding affinity for **3CL^{pro}**, which surpassed that of the reference inhibitors, as presented in Table 2. Remarkably, all the ligands had excellent binding stability, occupying the active site in varying ways at the N3 binding site of **3CL^{pro}**, as exhibited in ESI S6 and Fig. S3 (ESI†).

Both the controls and the ligands bind to the active site of the **3CL^{pro}**, which majorly interacted with the residues through hydrogen bonding (HB) and non-covalent interactions. The result showed that N3 interacted *via* the conventional HB to His A:41, GLU A:166, ASP A:187, and GLN A:189, accompanied with various non-covalent interactions, *i.e.*, MET A:49, LEU A:50, ASN A:142, and PRO A:168. It was noticed that the N3 docked complex is stabilized by HB interactions at the catalytic dyad HIS A:41. Further, the Chloroquine and Remdesivir docked complex suggested that these complexes are also stabilized by HB and hydrophobic interaction at the catalytic dyad of **3CL^{pro}**. Both Chloroquine and Remdesivir interacted with catalytic dyad CYS A:145. Accordingly, we can also accomplish like others that the binding of N3, Chloroquine, and Remdesivir to the catalytic residues of HIS A:41and CYS A:141 of **3CL^{pro}** may be an essential key beside the inhibition of its protease activity.

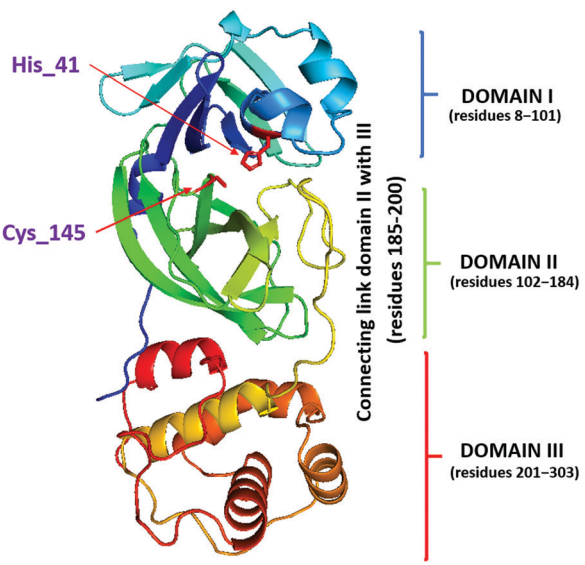

Fig. 3 Ribbon structure representation of SARS-CoV-2 main protease (PDB ID: 6LU7) with its domains.

As the highest docked compound, compound **4d** interacted with the both of the catalytic dyad of **3CL^{pro}** through HB interaction formed by CYS A:145 and the hydroxyl group (–OH) and pi–sigma interaction formed by HIS A:41 and acetyl group ($-CH_3$) of compound **4d**, as presented in Table 2 and Fig. 4. Moreover, its interaction is observed to be consistent with that of the used positive controls, *i.e.*, N3, Chloroquine, and Remdesivir. Compound **4a**, **4b**, **4c**, and **4e** have also interacted with one or both of the catalytic dyads of **3CL^{pro}** through HB and/or hydrophobic interactions. Generally, it is worth highlighting that all the synthesized ligand-docked complexes are stabilized by HB or non-covalent interactions to one or both the residues of the catalytic dyad of **3CL^{pro}**. This confirms that **4a** and its derivatives may serve as a potential inhibitor candidate against **3CL^{pro}** of SARS-CoV-2. All of the 2D and 3D representations of the investigated compounds are presented in ESI S7 and S8 (ESI†).

Generally, we found that HB and hydrophobic interactions were the most frequently observed in these studied protein–ligand complexes. In biological complexes, HBs are influential directional intermolecular interactions and play a major role in the specificity of molecular recognition.[62,63] Previously, it is already known that the main driving force in drug–receptor interactions is the hydrophobic interactions.[64] The densest clusters are those formed by aromatic carbon in the ligands and aliphatic carbon in the receptors. It is interesting to note that the existence of aromatic rings is an important key in the inhibition of small molecules. Interestingly, the aromatic ring system is the most effective, with benzene being the most common ring system, against about 76% of the approved drugs.[65,66] Thus, not surprisingly, the synthesized **4a** and its derivatives along with N3, Chloroquine, and Remdesivir side-chains are frequently involved in hydrophobic interactions.

Drug-likeness prediction and ADMET analysis. Further, to get an insight about the pharmacokinetic parameters, the synthesized **4a** and its derivatives along with Chloroquine, Remdesivir, and N3 were screened following Lipinski's rule of five[67] using SWISSADME server. This rule describes the principle of molecular properties for a drug's pharmacokinetics in the human body, *i.e.*, ADMET is represented as radar representation, as exhibited in ESI S9 and Fig. S6 (ESI†). The red area of the radar plot characterizes "good" oral bioavailability whereas the red bold line signifies

Table 2 Interacting amino acid residues of **3CL^{pro}** of SARS-CoV-2 with the synthesized compounds **4a–e** along with N3, Chloroquine, and Remdesivir

Complexes	Binding energy (kcal mol^{-1})	H-bond	Other interacted residues
4a	−7.6	LEU A:141, GLY A:143, SER A:144, CYS A:145, HIS A:163, MET A:165, GLU A:166, ARG A:188	—
4b	−7.1	ASN A:142, GLY A:143, CYS A:145, ARG A:188	LEU A:27, HIS A:41, MET A:49, MET A:165, PRO A:168
4c	−7.2	GLY A:143	HIS A:41, CYS A:145, GLU A:166
4d	−8.1	LEU A:141, SER A:144, CYS A;145, HIS A:163, MET A:165, GLU A:166, ARG A:188	HIS A:41
4e	−7.8	GLY A:143, MET A:165, GLU A:166, ARG A:188	CYS A:145, GLN A:189
N3	−7.5	His A:41, GLU A:166, ASP A:187, GLN A:189	MET A:49, LEU A:50, ASN A:142, PRO A:168
Chloroquine (antimalarial)	−5.7	LEU A:141, GLY A:143, CYS A:145, HIS A:163, MET A:165, GLU A:166, ARG A:188	—
Remdesivir (antiviral)	−7.8	LEU A:141, ASN A:142, GLY A:143, SER A:144, CYS A:145, HIS A:163, GLN A:189	MET A:49, MET A:165

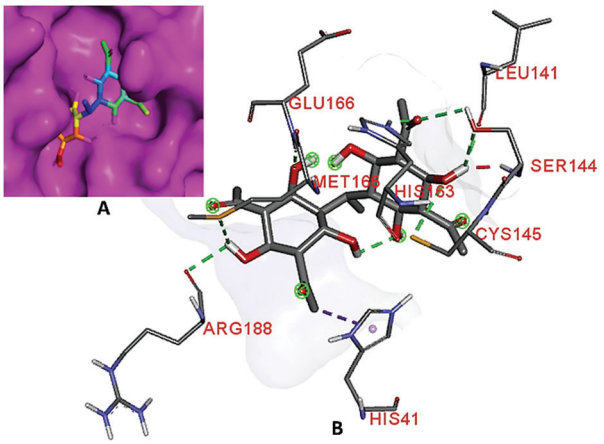

Fig. 4 3D positioning of compound **4d** inside the active pocket of **3CL^{pro}** (A), 3D representation of compound **4d** docked into the active pocket of **3CL^{pro}**, forming seven hydrogen bonds with LEU A:141, SER A:144, CYS A;145, HIS A:163, MET A:165, GLU A:166, ARG A:188 (B).

values of considered properties of the investigated molecule. As presented in Table 3, except Chloroquine, all of the synthesized compounds, N3, and Remdesivir obeyed Lipinski's rule. Compounds **4b**, **4c**, and **4e** obeyed Lipinski's rule in the number of HB and the molecular weight. N3 suffered from a number of rotatable bonds and molecular weight. Accordingly, the violation of 2 or more of compounds **4b**, **4c**, **4e**, N3, and Remdesivir predicts a molecule as a non-orally available drug. However, because of the high polarity value of these compounds, they could be given intravenously. Notably, compound **4a** and **4d** satisfied the criteria of Lipinski's rule with a slight deviation in the number of HB.

Afterwards, to predict the absorption level of the synthesized **4a** and its derivatives, intestinal absorption (human), Caco-2 permeability, and P-glycoprotein substrate or inhibitor was employed. Among the synthesized compounds, compound **4d** and **4e** are characterized by the higher value of Caco-2, as presented in Table 4. Besides, all the synthesized compounds are considered to be easily absorbed, which is indicated by the value of human intestinal absorption (HIA) no less than 30%. According to the BBB value, all of the synthesized compounds also revealed that these mentioned molecules are poorly distributed in the brain. In addition, the toxicity prediction (Table 4) revealed that all the investigated compounds displayed negative AMES toxicity, which is classified as non-carcinogenic. These *in silico* studies were fairly matched as compared with the previous literature.[17] Compound **4a** derivatives, particularly for analogue compound **4e**, showed good anti-HIV activity. This compound showed an IC_{50} of 0.28 μM and a CC_{50} of 3.15 μM, representing a good safety index for further study as a potential lead molecule.

Prediction of the activity spectra. A portion of the envisaged biological activity, particularly the antiviral activities for **4a** and its derivatives along with N3, Chloroquine, and Remdesivir as the references, are given in ESI S10 and Table S2 (ESI†). This result is mainly reported as the list of antiviral activities along with a suitable Pa and Pi ratio, which approximates the possibility for the investigated compound to be active and inactive, respectively. Accordingly, **4a** and its derivatives revealed various antiviral properties compared to the used references, which means that these compounds are better than compound N3, Chloroquine, and Remdesivir.

Table 3 Physicochemical properties of the synthesized compounds **4a–e** along with N3, Chloroquine, and Remdesivir

Lipinski filters	4a	4b	4c	4d	4e	N3	Chloroquine	Remdesivir
MW (g mol^{-1})	432.4	544.6	600.7	446.4	508.47	680.8	319.9	602.6
RB	6	10	14	6	7	22	8	14
HBA	10	10	10	10	10	9	2	12
HBD	6	6	6	6	6	5	1	4
TPSA (Å^2)	189.7	189.7	189.7	189.7	189.7	197.8	28.16	213.4
c log *P*	1.42	3.74	5.09	1.88	2.43	2.69	−4.15	1.50
MR.	108.8	147.3	166.5	113.6	133.3	184.1	97.41	150.43
Viol.	1	2	2	1	2	2	0	2

Table 4 Pharmacokinetic (ADMET) properties of the synthesized compounds **4a–e** along with N3, Chloroquine, and Remdesivir

Absorption (Probability)	**4a**	**4b**	**4c**	**4d**	**4e**	N3	Chloroquine	Remdesivir
BBB	BBB+ (0.7166)	BBB+ (0.6237)	BBB+ (0.6526)	BBB+ (0.6785)	BBB+ (0.6785)	BBB− (0.9070)	BBB+ (0.7421)	BBB− (0.7452)
HIA (%)	53.976	51.987	54.998	56.057	63.356	57.19	89.95	71.109
Bio. score	0.55	0.17	0.17	56.057	0.17	0.17	0.55	0.17
Caco-2 Permeability	Caco2+ (0.6910)	Caco2+ (0.6816)	Caco2+ (0.6690)	Caco2+ (0.8071)	Caco2+ (0.8071)	Caco2− (0.6946)	Caco2+ (0.5804)	Caco2− (0.6599)
P-glycoprotein Substrate	Yes	No	Yes	Yes	Yes	Yes	Yes	Yes
P-glycoprotein I inhibitor	No	No	Yes	No	No	Yes	No	No
P-glycoprotein II inhibitor	No	No	Yes	No	Yes	No	No	No
Renal organic cation transporter	Non-inhibitor (0.9054)	Non-inhibitor (0.9013)	Non-inhibitor (0.9079)	Non-inhibitor (0.9126)	Non-inhibitor (0.9126)	Non-inhibitor (0.6722)	Inhibitor (0.8743)	Non-inhibitor (0.9576)
Distribution (probability)								
Subcellular localization	Mitochondria (0.8747)	Mitochondria (0.9013)	Mitochondria (0.8748)	Mitochondria (0.8814)	Mitochondria (0.8814)	Mitochondria (0.6722)	Lysosome (0.8743)	Lysosome (0.3774)
Metabolism								
CYP2D6 substrate	No	No	No	No	No	No	Yes	No
CYP3A4 substrate	No	No	No	No	No	Yes	Yes	Yes
CYP1A2 inhibitor	No	No	No	No	Yes	No	No	No
CYP2C19 inhibitor	No	No	No	No	No	No	No	No
CYP2C9 inhibitor	No	No	No	No	Yes	Yes	No	No
CYP2D6 inhibitor	No	No	No	No	No	No	Yes	No
CYP3A4 inhibitor	No	No	No	No	No	Yes	No	No
Toxicity								
AMES toxicity	Non-AMES toxic (0.9298)	Non-AMES toxic (0.9332)	Non-AMES toxic (0.8622)	Non-AMES toxic (0.9689)	Non-AMES toxic (0.9689)	Non-AMES toxic (0.6802)	Non-AMES toxic	Non-AMES toxic (0.6158)
Carcinogens	Non-carcinogens (0.8195)	Non-carcinogens (0.8158)	Non-carcinogens (0.8340)	Non-carcinogens (0.7782)	Non-carcinogens (0.7782)	Non-carcinogens (0.8575)	Non-carcinogens	Non-carcinogens (0.8293)
Acute oral toxicity	III (0.7664)	III (0.7928)	III (0.6395)	IV (0.8013)	III (0.8013)	III (0.6034)	II (0.7370)	III (0.5361)
Rat acute toxicity LD50, mol kg^{-1}	2.4036	2.3482	2.6990	2.3990	2.3990	2.5188	2.9547	2.7169
log *S* (ESOL)	−4.08	−7.08	−7.70	−4.37	−5.48	−4.89	−4.55	−4.12
Pharmacokinetics								
GI absorption	Low	Low	Low	Low	Low	Low	Low	Low
log K_p (cm s^{-1})	−7.06	−4.78	−4.49	−6.91	−6.48	−8.07	−4.96	−8.62

DFT study. Through the DFT study, it is possible to establish the correlation between the molecular structure and the experimental results, which provides some essential and crucial data on the structure and reactivity from the molecular perspective.[68,69] The value of HOMO, LUMO, ΔE_{gap}, I, and A of the investigated compounds as the computed quantum chemical parameters are presented in ESI S13 and Table S3 (ESI†). The HOMO and LUMO values are depicted by its electron-donating and receiving ability, respectively, and are two key well-established aspects prompting the bioactivities and reactivity of a molecule or a bioactive compound.[70,71]

In this work, the HOMO calculated energies of the **4a** and its derivatives (−6.63 to −6.54 eV) are comparable with that of N3 (−6.50 eV) and Chloroquine (−6.24 eV). However, their LUMO energies (ranged from −2.16 to −2.27 eV) were observed only at the same level as that of N3 (−2.23 eV). The ΔE_{gap} of **4a** and its derivatives also revealed more stability (therefore less activity) than N3.

Notably, the level of LUMO energy has shown an essential impact on the increase in the reactivity of **4a** and its derivatives along with the existing references. Moreover, the shape and placement of the LUMO orbital should be considered. Previously, there are many studies that have revealed that the biological activity of the molecules is determined by the placement of the LUMO orbitals together with their energies.[72] Fig. 5A represents the frontier molecular orbital (FMO) shapes for compound **4d** and N3. The HOMO is mostly localized on the aromatic ring, carbonyl, and hydroxyl groups for compound **4d** and the pyrrolidine ring for N3. On the contrary, in both the cases, the empty LUMO orbital is delocalized over the entire molecule. The determination of the two parameters such as I and A is also important, which allows us to measure the global reactivity descriptors.

Furthermore, we also determined the other quantum chemical such as ηS, χ, μ, and ω, which are essential to describe the reactivity and stability of the investigated compounds, as presented in ESI S13 and Table S3 (ESI†). According to ESI S13 and Table S3 (ESI†), it was observed that all the synthesized compounds, along with Chloroquine and Remdesivir, are characterized by the higher value of η than that of N3. This indicates that these compounds are more stable than N3 as the reference. Further, the values of S, χ, μ, and ω also signify that the reactivity for **4a** and its derivatives is higher than that for N3, Chloroquine, and Remdesivir, which fairly matched with the molecular docking findings.

Afterwards, the MEP map was established to provide identification and prediction about the reactive sites for nucleophilic and electrophilic attacks of the investigated compounds and further explanation to know the processes of biological recognition and interactions of HB,[73] as depicted in Fig. 5B. The map depicts negative electrostatic potential regions (red) of compound **4d** mostly centered over the carbonyl functional groups of the acyl moiety, while the methyl groups of the acyl moiety and aromatic rings represent the positive regions (blue). For N3, the negative electrostatic potential regions are mostly focused over the oxygen atoms of carbonyl groups while the positive values are centered over the N atoms. The MEP maps of all the synthesized compounds along with the references are given in ESI S12 and Fig. S8 (ESI†).

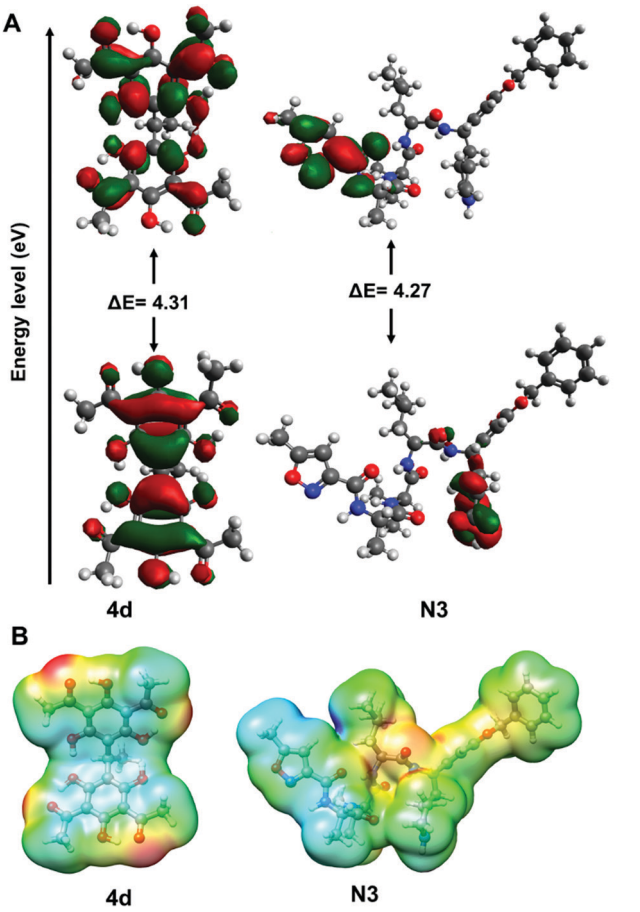

Fig. 5 HOMO and LUMO plots of compound **4d** and N3. Positive and negative phases are shown in red and green colors, respectively (**A**). MEP maps of compound **4d** (left) and N3 (right). The values of electrostatic potential are illustrated with different colors, which increase in the order red < orange < yellow < green < blue (**B**).

SAR study. The SAR of the synthesized **4a** and its derivatives is derived from their binding affinities to the **3CL^{pro}** active site in order to designate the role of the substituents present in **4a** compounds. This privileged scaffold **4a** comprises three main functionalities, *i.e.*, aromatic, hydroxyl, and acyl groups, as displayed in Fig. 6. First, the role of the substituents at the R1 position was studied. The presence of longer substituents than methyl such as butyryl (**4b**) and valeryl (**4c**) chains makes them structurally them less active, which was marked from the higher binding energies in the same case of interaction. On the contrary, the lower binding energy and a higher number of HB interactions of compound **4d** (−8.1 kcal mol^{-1}) and **4a** (−7.6 kcal mol^{-1}) can be assigned to the less steric hindrance due to the presence of methyl substituents at the R1 position. This observation was in good agreement with the *in vitro* evaluation by Chauthe *et al.* in 2012.[15] They revealed that compound **4a** and **4d** secured better anticancer activity against Calu-1 than compound **4b** and **4c**. These results clearly specified the importance of the alkyl length at the R1 position affecting the biological activity of **4a** derivatives.

Then, we noticed that the interaction between compound **4a–d** and the catalytic dyad CYS A:145 of **3CL^{pro}** was facilitated

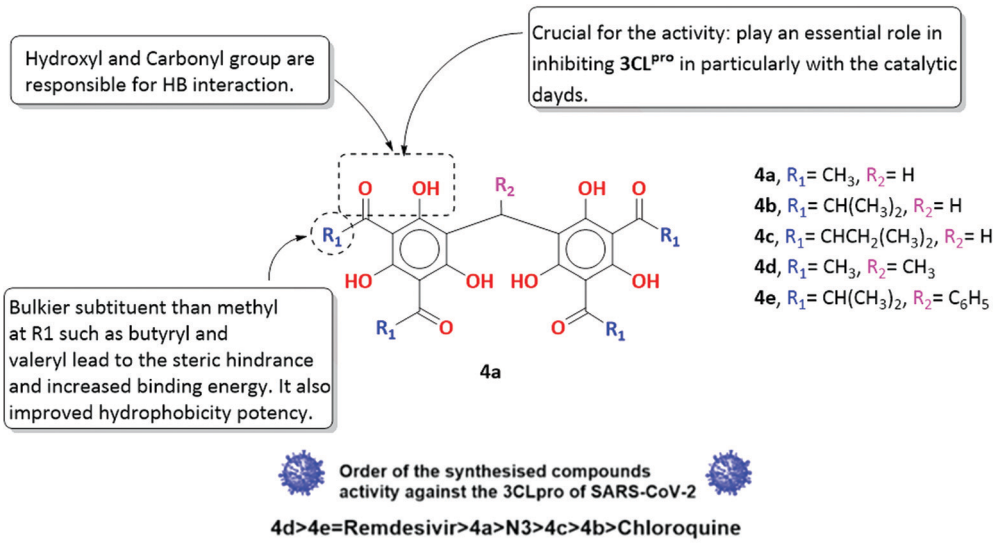

Key findings for mechanistic insights

1. Compound **4d** exhibited the most potent inhibitory against the 3CL^{pro} of SARS-CoV-2 with a binding energy 8.1 (Kcal/mol). The interactions were formed by seven strong hydrogen bonds with LEU A:141, SER A:144, CYS A;145, HIS A:163, MET A:165, GLU A:166, ARG A:188.
2. Docking studies reveal that the compound **4d** interacted with both of catalytic dyads of 3CL^{pro} (HIS A:41 and CYS A:145).
3. The introduction of longer substituent such as butyryl (**4b**) and valeryl chain (**4c**) than methyl at **R1** causing them less active.
4. The presence of phenyl at **R2** made the interaction with catalytic dyad CYS A:145 favoured to be with the aromatic ring system (**R2**) through pi-alkyl interaction instead of with the hydroxyl or carbonyl group at the phloroglucinol system as compound **4a**-**4d** demonstrated.

Fig. 6 Structure–activity relationship of the synthesized compounds **4a–e** against **3CL^{pro}**.

through the hydroxyl or carbonyl group of the phloroglucinol ring. On the other hand, any interactions between the synthesized compounds with the catalytic dyad HIS A:41 was facilitated through pi–alkyl interaction for compound **4b**, **4c**, and **4e**, whereas it was through pi-sigma interaction for compound **4d**. In the case of phenylene ring substituting the methylene bridge (R2), compound **4e** exhibited a lower binding energy (-7.8 kcal mol^{-1}) than that of compound **4a**. The result of the interaction with compound **4e** was surprising; the interaction with catalytic dyad CYS A:145 was favored with the aromatic ring system through pi–alkyl interaction instead of with the hydroxyl or carbonyl group at the phloroglucinol system. Moving to methyl as the substituent at position R2, compound **4d**, the lowest binding energy may be attributed to the existence of additional interaction with both the catalytic dyad of **3CL^{pro}**, *i.e.*, CYS A:145 and HIS A:41. Hence, with respect to the basis of molecular docking, ADMET properties, and SAR analysis, compound **4d** was labelled as the most considered analogue for further study.

Conclusions

To summarize the above studies, we have successfully demonstrated an efficient and eco-friendly route for the synthesis of **4a** derivatives over a superior heterogeneous **SSA** catalyst. The demonstration of the present US method (Method E) significantly shows magnificent benefits, both in terms of the sustainability and efficiencies compared to previous literatures, which has been assessed using EATOS software, Andraos algorithm, and energy requirement calculation. From the protein–ligand docking analysis, our findings confirmed that compound **4d** displayed a remarkable inhibition ability with the binding energy of -8.1 kcal mol^{-1}, which clearly showed that it may suppress **3CL^{pro}** by binding at both the catalytic dyad at the CYS A:145 and HIS A:41 residue, along with the highly conserved substrate-recognition pocket of the SARS-CoV-2 with N3 as a native inhibitor. Besides, our designed compounds also revealed good pharmacokinetic and toxicological properties. Finally, due to the suitable docking result and pharmacotherapeutic profile, we recommend our most promising compound as well as **4d** for further assessment, *i.e.*, *in vitro* and *in vivo* to reach an effective therapy so as to inhibit the **3CL^{pro}** enzyme of this viral disease.

Conflicts of interest

There are no conflicts to declare.

Acknowledgements

This work was supported by the Institute of Research and Community of Services Sebelas Maret University for finance

through Hibah Penelitian Unggulan (PU-UNS) 2020 (452/UN27.21/PN/2020). The authors are thankful to Viardy Kurniansyah, S. Si., for his contribution to geometry optimization. We are also grateful to Heri Purnomo, S. Si., and Miracle Sadrini, S. Si., for helpful discussions about molecular docking studies.

Notes and references

1 C. C. Lai, T. P. Shih, W. C. Ko, H. J. Tang and P. R. Hsueh, *Int. J. Antimicrob. Agents*, 2020, **55**, 105924.
2 D. Kaul, *Curr. Med. Res. Pract.*, 2020, **10**, 54–64.
3 D. S. Hui, E. I. Azhar, T. A. Madani, F. Ntoumi, R. Kock, O. Dar, G. Ippolito, T. D. Mchugh, Z. A. Memish, C. Drosten, A. Zumla and E. Petersen, *Int. J. Infect. Dis.*, 2020, **91**, 264–266.
4 S. A. Rasmussen, *Ann. Oncol.*, 2020, 19–21.
5 Z. Jin, X. Du, Y. Xu, Y. Deng, M. Liu, Y. Zhao, B. Zhang, X. Li, L. Zhang, C. Peng, Y. Duan, J. Yu, L. Wang, K. Yang, F. Liu, R. Jiang, X. Yang, T. You, X. Liu, X. Yang, F. Bai, H. Liu, X. Liu, L. W. Guddat, W. Xu, G. Xiao, C. Qin, Z. Shi, H. Jiang, Z. Rao and H. Yang, *Nature*, 2020, **582**, 289–293.
6 D. Bhowmik, R. Nandi, R. Jagadeesan, N. Kumar, A. Prakash and D. Kumar, *Infect., Genet. Evol.*, 2020, **84**, 104451.
7 P. Sang, S. H. Tian, Z. H. Meng and L. Q. Yang, *RSC Adv.*, 2020, **10**, 15775–15783.
8 J. Wang, *J. Chem. Inf. Model.*, 2020, **60**, 3277–3286.
9 A. A. Zaki, A. A. Al-Karmalawy, Y. A. El-Amier and A. Ashour, *New J. Chem.*, 2020, **44**, 16752–16758.
10 D. J. Newman and G. M. Cragg, *Future Med. Chem.*, 2009, **1**, 1415–1427.
11 D. G. Kingston and D. J. Newman, *IDrugs*, 2005, **8**, 990–992.
12 A. M. Sayed, A. R. Khattab, A. M. AboulMagd, H. M. Hassan, M. E. Rateb, H. Zaid and U. R. Abdelmohsen, *RSC Adv.*, 2020, **10**, 19790–19802.
13 A. E. Allam, H. K. Assaf, H. A. Hassan, K. Shimizu and Y. A. M. M. Elshaier, *RSC Adv.*, 2020, **10**, 29983–29998.
14 I. P. Singh, J. Sidana, S. B. Bharate and W. J. Foley, *Nat. Prod. Rep.*, 2010, **27**, 393.
15 S. K. Chauthe, S. B. Bharate, G. Periyasamy, A. Khanna, K. K. Bhutani, P. D. Mishra and I. P. Singh, *Bioorg. Med. Chem. Lett.*, 2012, **22**, 2251–2256.
16 P. Gupta, R. Kumar, P. Garg and I. P. Singh, *Bioorg. Med. Chem. Lett.*, 2010, **20**, 4427–4431.
17 S. K. Chauthe, S. B. Bharate, S. Sabde, D. Mitra, K. K. Bhutani and I. P. Singh, *Bioorg. Med. Chem.*, 2010, **18**, 2029–2036.
18 I. Pal Singh and S. B. Bharate, *Nat. Prod. Rep.*, 2006, **23**, 558.
19 M. O. Duarte, S. Lunardelli, C. J. Kiekow, A. C. Stein, L. Müller, E. Stolz, S. M. K. Rates and G. Gosmann, *Nat. Prod. Commun.*, 2014, **9**, 671–674.
20 L. Mammino, *J. Mol. Struct.*, 2019, **1176**, 488–500.
21 S. B. Bharate, R. Mudududdla, J. B. Bharate, N. Battini, S. Battula, R. R. Yadav, B. Singh and R. A. Vishwakarma, *Org. Biomol. Chem.*, 2012, **10**, 5143.
22 P. T. Anastas and J. C. Warner, *Principles of green chemistry*, Oxford University Press, New York, 1998.
23 M. Arisawa, A. Fujita, N. Morita and S. Koshimura, *Planta Med.*, 1990, **56**, 377–379.
24 X. J. Qin, M. Y. Feng, H. Liu, W. Ni, T. Rauwolf, J. A. Porco, H. Yan, L. He and H. Y. Liu, *Org. Lett.*, 2018, **20**, 5066–5070.
25 A. V. Pinhatti, F. M. C. De Barros, C. B. De Farias, G. Schwartsmann, G. L. V. Poser and A. L. Abujamra, *Anti-cancer Drugs*, 2013, **24**, 699–703.
26 V. Belekar, A. Shah and P. Garg, *Mol. Diversity*, 2013, **17**, 97–110.
27 M. A. Zolfigol, *Tetrahedron*, 2001, **57**, 9509–9511.
28 R. M. N. Kalla, S. S. Reddy and I. Kim, *Catal. Lett.*, 2019, **149**, 2696–2705.
29 M. Firdaus and M. D. Prameswari, *Bull. Chem. React. Eng. Catal.*, 2019, **14**, 9.
30 J. Hagen, I. Chorkendorff and J. W. Niemantsverdriet, *Concepts of Modern Catalysis and Kinetics Catalysis from A to Z Principles and Practice of Heterogeneous Catalysis Catalytic Membranes and Membrane Reactors Spectroscopy in Catalysis*, 2006.
31 W. E. Prasetyo, T. Kusumaningsih and M. Firdaus, *Synth. Commun.*, 2019, **49**, 3352–3372.
32 M. Chtourou, A. Lahyani and M. Trabelsi, *React. Kinet., Mech. Catal.*, 2019, **126**, 237–247.
33 C. J. Ellstrom and B. Török, *Application of Sonochemical Activation in Green Synthesis*, Elsevier, 2018.
34 M. L. Cheney, G. J. McManus, J. A. Perman, W. Zhenqiang and M. J. Zaworotko, *Cryst. Growth Des.*, 2007, **7**, 616–617.
35 M. L. Cheney, M. J. Zaworotko, S. Beaton and R. D. Singer, *J. Chem. Educ.*, 2008, **85**, 1649–1651.
36 J. K. Awalt, P. J. Scammells and R. D. Singer, *ACS Sustainable Chem. Eng.*, 2018, **6**, 10052–10057.
37 J. G. Hernández and C. Bolm, *J. Org. Chem.*, 2017, **82**, 4007–4019.
38 T. Kusumaningsih, M. Firdaus, M. W. Wartono, A. N. Artanti, D. S. Handayani and A. E. Putro, *IOP Conf. Ser.: Mater. Sci. Eng.*, 2016, **107**, 012059.
39 T. Kusumaningsih, M. Firdaus, A. N. Artanti and W. E. Prasetyo, *IOP Conf. Ser.: Mater. Sci. Eng.*, 2019, **578**, 012057.
40 C. Hertiningtyas, T. Kusumaningsih and M. Firdaus, AIP Conference Proceedings, AIP Publishing LLC, 2020, vol. 2237, p. 20018.
41 M. Eissen and J. O. Metzger, *Chem. – Eur. J.*, 2002, **8**, 3580–3585.
42 J. Andraos, *Org. Process Res. Dev.*, 2009, **13**, 161–185.
43 M. J. Gronnow, R. J. White, J. H. Clark and D. J. Macquarrie, *Org. Process Res. Dev.*, 2005, **9**, 516–518.
44 T. Kusumaningsih, W. E. Prasetyo and M. Firdaus, *RSC Adv.*, 2020, **10**, 31824–31837.
45 A. Minassi, L. Cicione, A. Koeberle, J. Bauer, S. Laufer, O. Werz and G. Appendino, *Eur. J. Org. Chem.*, 2012, 772–779.
46 T. D. Grayfer, P. Grellier, E. Mouray, R. H. Dodd, J. Dubois and K. Cariou.
47 K. Ramaiah, K. Srishailam, K. Laxma Reddy, B. V. Reddy and G. Ramana Rao, *J. Mol. Struct.*, 2019, **1184**, 405–417.
48 K. O. Rachedi, T. S. Ouk, R. Bahadi, A. Bouzina, S. E. Djouad, K. Bechlem, R. Zerrouki, T. Ben Hadda, F. Almalki and M. Berredjem, *J. Mol. Struct.*, 2019, **1197**, 196–203.

49 A. Allouche, *J. Comput. Chem.*, 2012, **32**, 174–182.
50 D. Gfeller, A. Grosdidier, M. Wirth, A. Daina, O. Michielin and V. Zoete, *Nucleic Acids Res.*, 2014, **42**, 32–38.
51 D. E. V. Pires, T. L. Blundell and D. B. Ascher, *J. Med. Chem.*, 2015, **58**, 4066–4072.
52 S. Parasuraman, *J. Pharmacol. Pharmacother.*, 2011, **2**, 52–53.
53 I. Artaki, T. W. Zerda and J. Jonas, *J. Non-Cryst. Solids*, 1986, **81**, 381–395.
54 F. A. Carey and R. J. Sundberg, *Advanced organic chemistry, part A: structure and mechanisms*, Springer, 2007, vol. 5.
55 D. Prat, A. Wells, J. Hayler, H. Sneddon, C. R. McElroy, S. Abou-Shehada and P. J. Dunn, *Green Chem.*, 2015, **18**, 288–296.
56 Y. Li, B. Yu and R. Wang, *Tetrahedron Lett.*, 2016, **57**, 1856–1859.
57 N. Baig RB and R. S. Varma, *An Introduction to Green Chemistry Methods*, Future Science Ltd, Unitec House, 2 Albert Place, London N3 1QB, UK, 2013, pp. 18–38.
58 M. J. Keiser, V. Setola, J. J. Irwin, C. Laggner, A. I. Abbas, S. J. Hufeisen, N. H. Jensen, M. B. Kuijer, R. C. Matos, T. B. Tran, R. Whaley, R. A. Glennon, J. Hert, K. L. H. Thomas, D. D. Edwards, B. K. Shoichet and B. L. Roth, *Nature*, 2009, **462**, 175–181.
59 K. Anand, J. Ziebuhr, P. Wadhwani, J. R. Mesters and R. Hilgenfeld, *Science*, 2003, **300**, 1763–1767.
60 K. Anand, G. J. Palm, J. R. Mesters, S. G. Siddell, J. Ziebuhr and R. Hilgenfeld, *EMBO J.*, 2002, **21**, 3213–3224.
61 V. Chandel, S. Raj, B. Rathi and D. Kumar, *Chem. Biol. Lett.*, 2020, **7**, 166–175.
62 E. Nittinger, T. Inhester, S. Bietz, A. Meyder, K. T. Schomburg, G. Lange, R. Klein and M. Rarey, *J. Med. Chem.*, 2017, **60**, 4245–4257.
63 T. Steiner, *Angew. Chem., Int. Ed.*, 2002, 41, 48–76.
64 R. Ferreira De Freitas and M. Schapira, *MedChemComm*, 2017, **8**, 1970–1981.
65 A. R. D. Taylor, M. Maccoss and A. D. G. Lawson, *J. Med. Chem.*, 2014, **57**, 5845–5859.
66 T. J. Ritchie and S. J. F. Macdonald, *J. Med. Chem.*, 2014, **57**, 7206–7215.
67 C. A. Lipinski, F. Lombardo, B. W. Dominy and P. J. Feeney, *Adv. Drug Delivery Rev.*, 2012, **64**, 4–17.
68 N. Flores-Holguín, J. Frau and D. Glossman-Mitnik, *Comput. Mol. Biosci.*, 2019, **09**, 41–47.
69 S. M. Hiremath, A. S. Patil, C. S. Hiremath, M. Basangouda, S. S. Khemalapure, N. R. Patil, S. B. Radder, S. J. Armaković and S. Armaković, *J. Mol. Struct.*, 2019, **1178**, 1–17.
70 A. Tariq, S. Nazir, A. W. Arshad, F. Nawaz, K. Ayub and J. Iqbal, *RSC Adv.*, 2019, **9**, 24325–24332.
71 S. Murugavel, C. Ravikumar, G. Jaabil and P. Alagusundaram, *J. Mol. Struct.*, 2019, **1176**, 729–742.
72 S. Tighadouini, S. Radi, F. Abrigach, R. Benabbes, D. Eddike and M. Tillard, *Novel β-keto-enol Pyrazolic Compounds as Potent Antifungal Agents. Design, Synthesis, Crystal Structure, DFT, Homology Modeling, and Docking Studies*, 2019, vol. 59.
73 C. Y. Panicker, H. T. Varghese, P. S. Manjula, B. K. Sarojini, B. Narayana, J. A. War, S. K. Srivastava, C. Van Alsenoy and A. A. Al-Saadi, *Spectrochim. Acta, Part A*, 2015, **151**, 198–207.